[redacted]

ANU-P/612
February, 1975.

ATOMIC AND SOLID STATE PHYSICS WITH THE 14UD

C.S. Newton

Department of Nuclear Physics,
The Australian National University,
Canberra, Australia

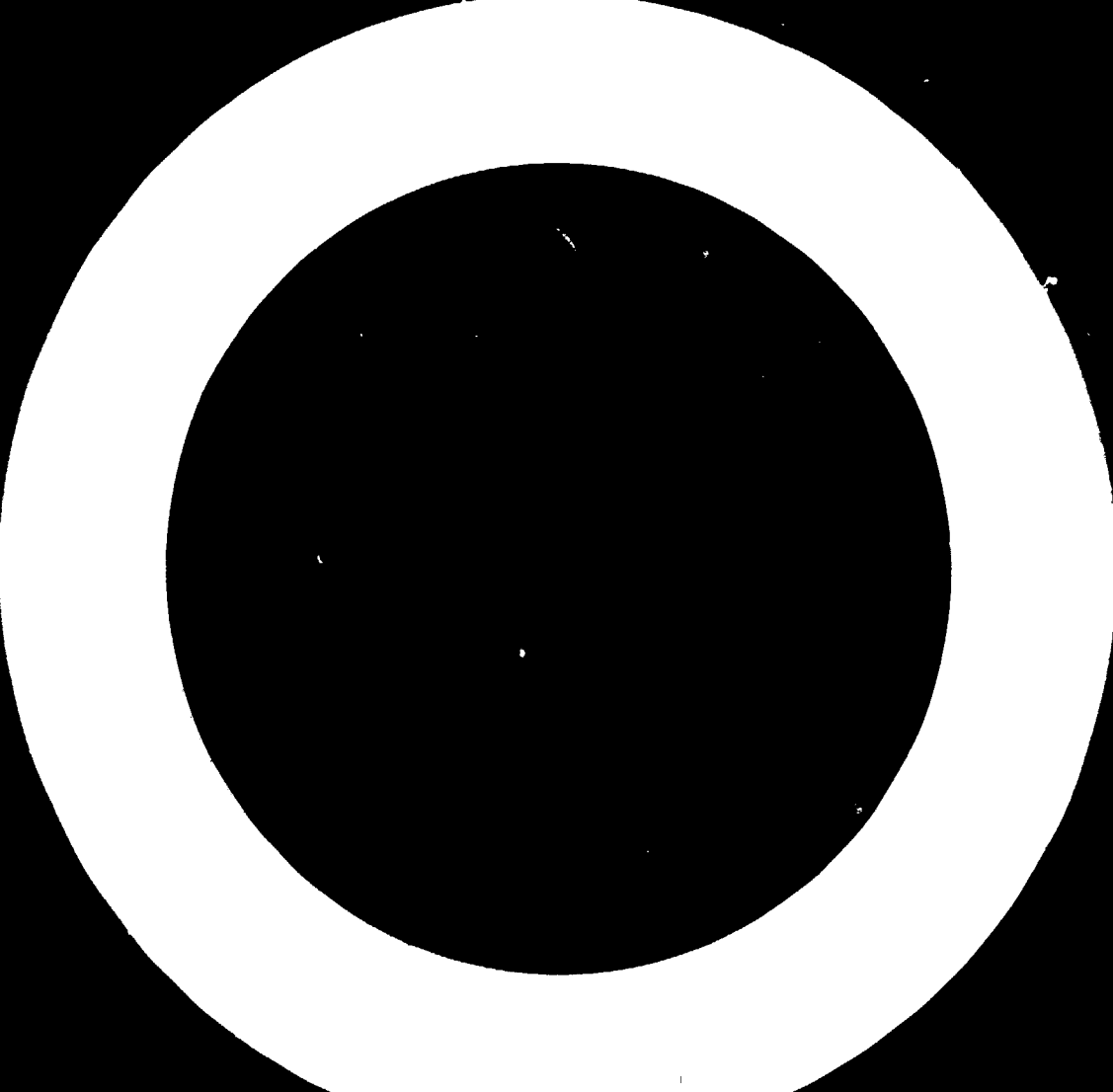

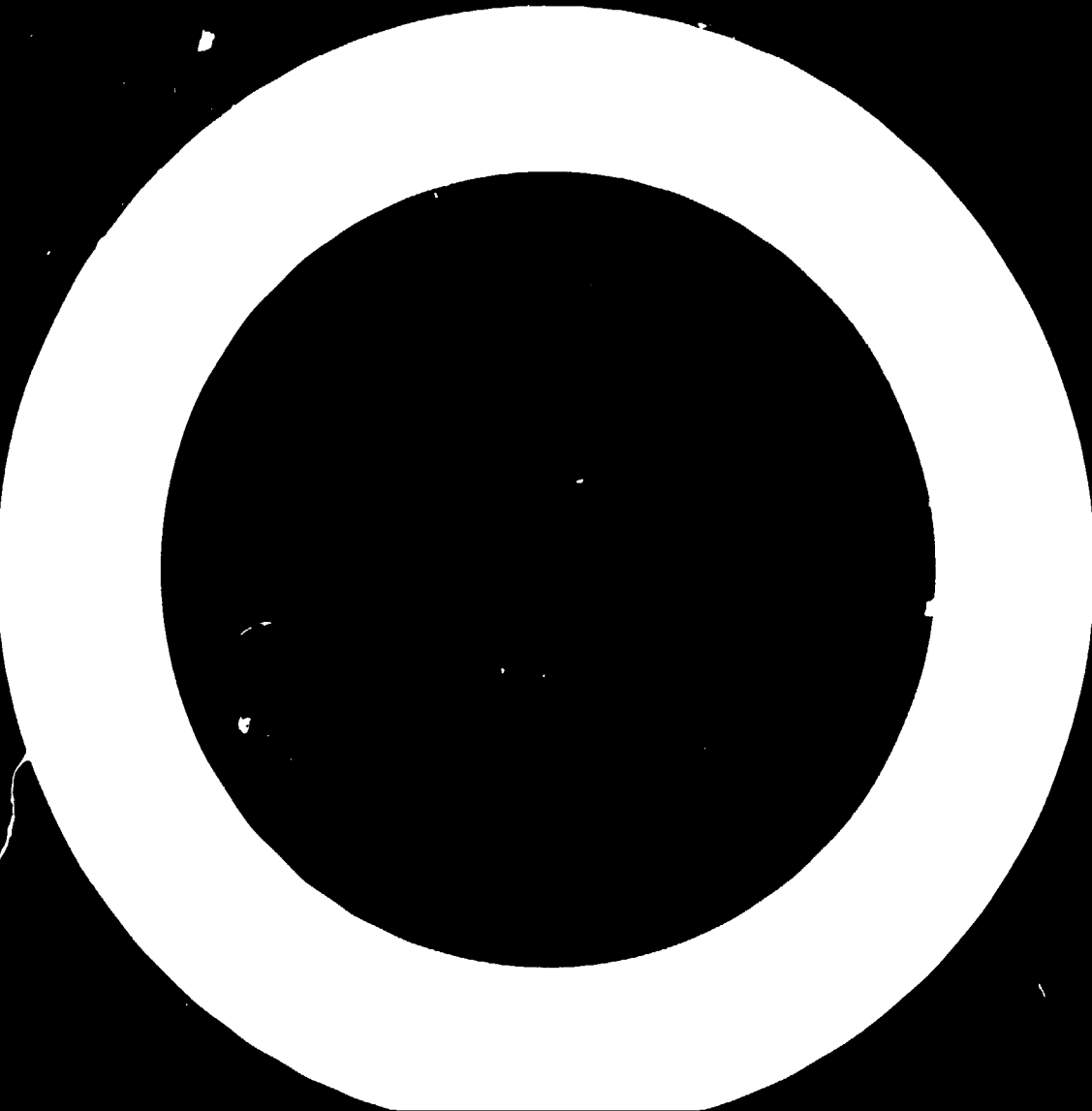

ATOMIC AND SOLID STATE PHYSICS WITH THE 14UD

C.S. Newton

§1. INTRODUCTION:

Not only will nuclear physics profit from the availability of energetic heavy ions, but also fields such as atomic physics, solid state physics, biology etc., where nuclear physics instrumentation can be implemented. In these notes I will point out a few aspects that are of interest for atomic and solid state physicists. As this report will be experimentally oriented the theories behind some of the experiments will be left to the reader to delve into on his own initiative.

The topics that will be mentioned here are as follows:

§2: Properties of excited ions
§3: Radiation damage studies by channeling
§4: Energy loss of ions, range measurements
§5: Oscillatory effects in channeling
§6: X-ray production in solids
§7: Coherence effects in channeling
§8: Formation of united atoms
§9: Proposal.

It can be noted at this point that beam-foil spectroscopy, as it is known here in the department is certainly not practicable on the 14UD accelerator. The reason for this is that ions of energies achievable by means of the 14UD accelerator are highly ionized and the atomic transitions will be in the low ångstrom wavelength range (corresponding to 50 eV - 100 keV range), and not in the visible range. As is shown in Table 1, continuous beam-foil studies necessitate using combinations of crystal spectrometers, and Si(Li) or Ge(Li) drifted detectors, not all of which are presently available in this department.

This report is based on a talk given in this department on 16th July 1973. The author thanks H.J. Hay and P.B. Treacy for their advice.

TABLE 1

SPECTRAL RANGE FOR ION-SOLID INTERACTIONS

The broad lines indicate the wavelength ranges which are accessible with the existing equipment in the department.

Wavelength (Å)	Energy (eV)	Analyzer + Detector	Detection Method
	1	Spectrometer + bolometer	Heat
10^4			
	10	Diffraction grating monochromator + photomultiplier	Photons
10^3			
	10^2	Grazing incidence monochromator + electron multipliers or channeltrons	Photons
10^2			
	10^3	Curved crystal spectrometers assisted by Gas flow proportional counters	Ionization
10			
	10^4	Si(Li) or Ge(Li) Detectors	Ionization
1			
	10^5		
0.1			

§2. PROPERTIES OF EXCITED IONS:

The scattering of energetic ions through a solid target generates a charge distribution of excited ions, which is energy dependent, and therefore one can study atomic t ansitions which are otherwise difficult to observe in the laboratory. It is possible u' n[illegible] the beam-foil source to assign atomic transitions to a specific charge state using the Doppler Shift technique[1], which cannot be achieved so directly with other sources, i.e. plasma physics. Up until the last few years only spectra of excited light ions have been measured extensively by the beam-foil source[2]. This has been partly due to the fact that for single ended high voltage accelerators, the ion source has put restrictions on the variety of ions one can accelerate. The heavy ions that one has been able to study have only been accelerated on low energy accelerators and therefore only neutral, singly ionized, and doubly ionized ionic spectra have been studied.

With the universal ion source combined with the accelerating potentials one can obtain on the 14UD accelerator, spectra of highly ionized heavy ions can be studied. Measured atomic transition probabilities are required since the knowledge of values of the atomic oscillator strength, f, is most unsatisfactory for the heavier elements, and is required for astrophysical problems. Lifetime measurement is the most straightforward approach for obtaining atomic transition probabilities, provided one can eliminate the problem of cascades into the level for which the decay is being studied. Less difficult problems of interpretation may arise from absorption, induced emission and de-exciting collisions.

Since, in the beam-foil source, all ions are excited at about the same position in space, and due to the magnetic selection of the projectile, which implies that the beam is monoenergetic, time measurements can be translated into spatial measurements.

The atomic structure of highly ionized heavy ions, especially hydrogen-like and helium-like are very interesting because the atomic electrons are pulled into substantially smaller radii. As pointed out by Wiese[3] one important aspect is f-value data for the highly ionized noble gas spectra, which is a convenient diagnostic tool in controlled thermonuclear fusion research. With the existing beam-foil equipment and Si(Li) detector and later with a crystal spectrometer these experiments can be performed on the 14UD accelerator. Other quantities that

are being studied at the moment are the Lamb-shift in hydrogenic ions[4,5] and the metastable auto-ionizing levels[6-10]. It has been known for some time that there are levels in the continuum that are metastable to auto-ionization and therefore can decay by photon emission. Knowledge about such metastable states is of astrophysical importance.

§5. RADIATION DAMAGE STUDIES BY CHANNELING:

The other line of research that is being done on the 2 MV accelerator can certainly be extended to the 14UD energy range. This is the study of ion-induced radiation damage in single crystals, in particular alkali halides. Alkali halides have been found to damage very quickly, when bombarded by light ions in the energy range of 0.5 MeV - 2.0 MeV[11,12]. It is hoped that the project will also include radiation damage of other solids. It is of technological interest to study radiation damage produced in single crystals by bombardment of heavy ions. For example the effects of implantation of boron, phosphorus and other ions into silicon and germanium are important for semi-conductor production.

One of the tools that is useful for these studies is the channeling effect[13-18], which is described briefly below. When a beam of charged particles impinges upon a solid target, Rutherford scattering, energy loss processes, etc. can occur and these processes all have cross-sections which depend on the impact parameter, which describes the characteristic distance in a collision between a beam particle and a target atom. In amorphous solids, which are assumed homogeneous and isotropic, the impact parameter distribution $\nu(b) = 2\pi b$ is independent of the orientation of the beam to the target, whereas in crystalline solids the situation is quite different. There the yields of reaction processes are found to be orientation dependent. Channeling is the process which describes that, in certain orientations of the crystal the particle has a greater probability of penetrating much further into the crystal than in an amorphous solid.

This enhanced penetration has been ascribed to the fact that the particle will, with high probability, suffer a small angle scattering as it passes close to a string of atoms in the crystal. The consequent steering effect will cause the particles to follow

trajectories which oscillate to and fro in the channel, as shown in Fig. 1. Under these conditions, the yields of close encounter processes are sharply reduced (Fig. 2.). From this, one obtains an important parameter for channeling, χ, which is the ratio of the yield of a process in a crystal in a specific orientation, Y_θ, to the yield of the same process performed in a hypothetical amorphous solid, Y_R. When the beam is aligned with a crystallographic axis or plane then χ will have a minimum, denoted by χ_{min}. One can use this parameter to describe how "perfect" a crystal is, and it is this parameter that has been used to monitor radiation damage,

$$\chi_{min} = \frac{Y_{ch}}{Y_R} = \pi Nd(a^2 + \langle\delta\rangle^2) \quad , \qquad 1.$$

where R denotes an orientation in the crystal which is assumed to give the same yield as in an amorphous solid. N is the atomic density, d is the interatomic spacing, a = Thomas-Fermi screening distance and δ is the thermal vibrational amplitude. The other parameter is ψ_c, defined as the transition angle between channeling and non-channeling. It is given by

$$\psi_c = a\sqrt{\frac{2Z_1 Z_2 e^2}{E \cdot d}} \quad , \qquad 2.$$

where E is the energy of the projectile with charge Z_1, and d is the atomic spacing in the crystal of atoms with charge Z_2. If the relative angle between the beam and a major crystallographic axis is less than the critical angle ψ_c then there is a large probability of channeling. For 2 MeV He^+ ions in silicon, the critical angle $\psi_c \approx 1°$ for axial channeling and $\approx 0.3°$ for planar channeling. The experiments to date which have been performed in this laboratory are measurements of χ_{min} for Rutherford scattering as a function of dose[12], shown in Fig. 3a. The projectiles were 1 MeV He^+ ions and the target crystals were NaCl, KCl, and LiF. By measuring the back scattered spectrum of He^+ ions from the crystal and taking the ratio of the yield to the random yield, one is able to deduce χ_{min} for a range of depths, thus determining the radiation damage in the crystal at different depths, Fig. 3b. The depth resolution depends on the energy resolution of the detection system. As shown in Fig. 3a a maximum is observed at a dose of $\sim 5 \times 10^{15}$ particles/cm^2 implying that the disorder created initially begins to 'anneal' out at higher doses.

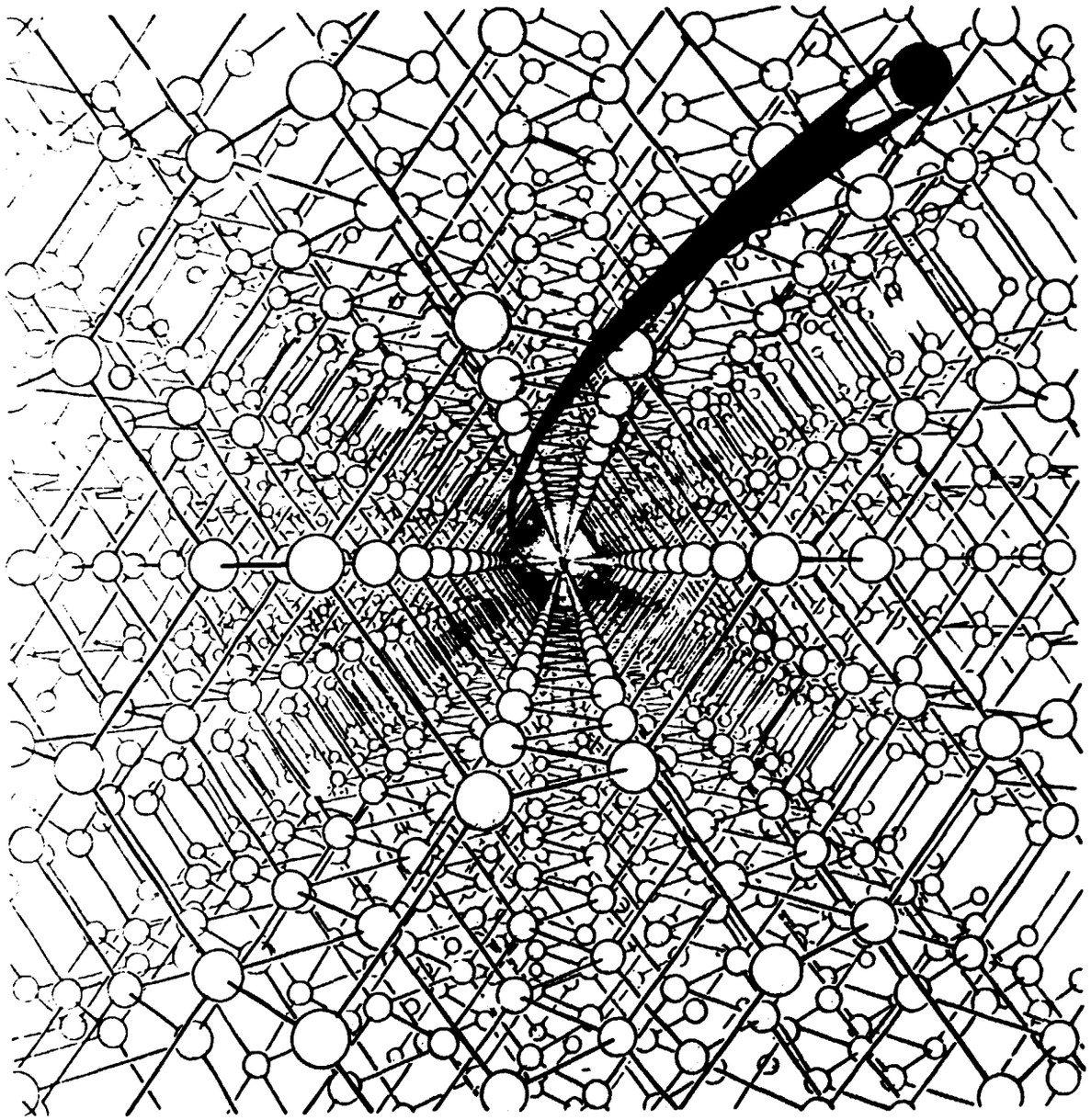

Fig. 1.

Point-blank view down the axis of a channel in a diamond-like crystal lattice shows the spiral path followed by a typical channeling particle. The distance covered by the particle in one turn of the spiral path is of the order of 100 interatomic distances, (Brandt, Ref.19).

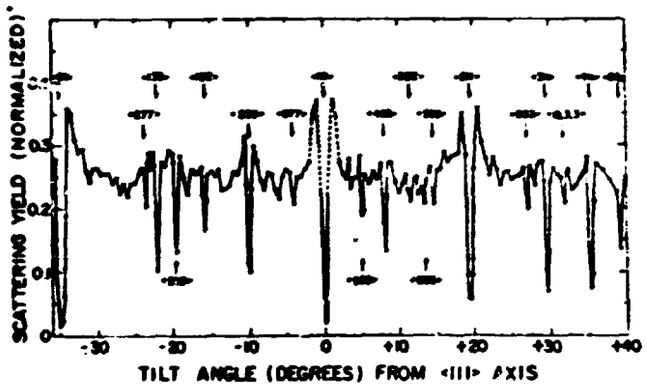

Fig. 2.

High-index axial channeling effects for 1.0-MeV helium in the {110} plane of silicon. The measured yield is from a scattering zone about 1000 Å beneath the crystal surface, (Davies, Ref.21).

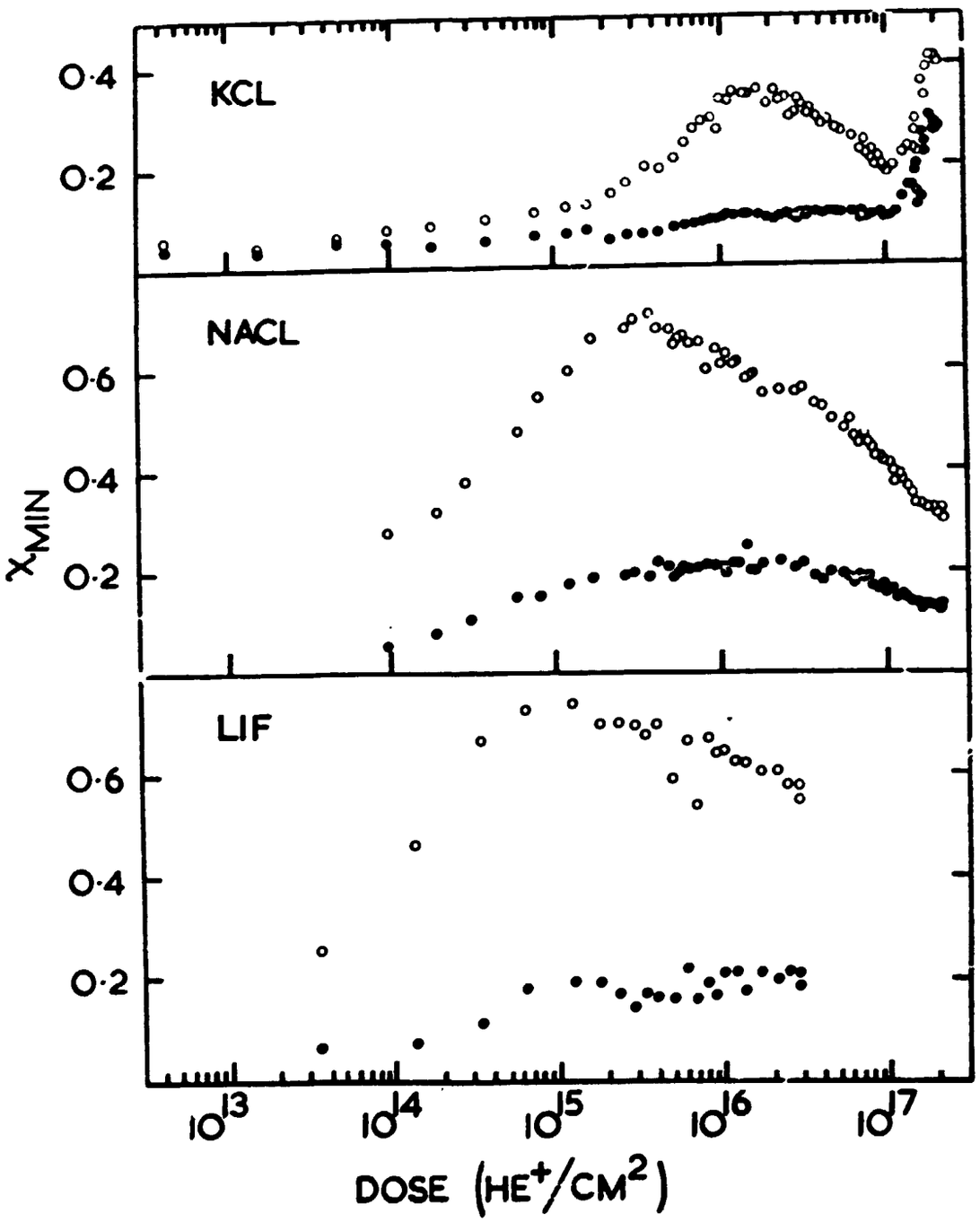

Fig. 3a.

χ_{min} (<100>) for 1 MeV He^+ ion scattering from the crystal surface (•) (extrapolated) and from a depth of 0.3 μm (○), (M.J. Hollis, C.S. Newton and P.B. Price, Ref. 12).

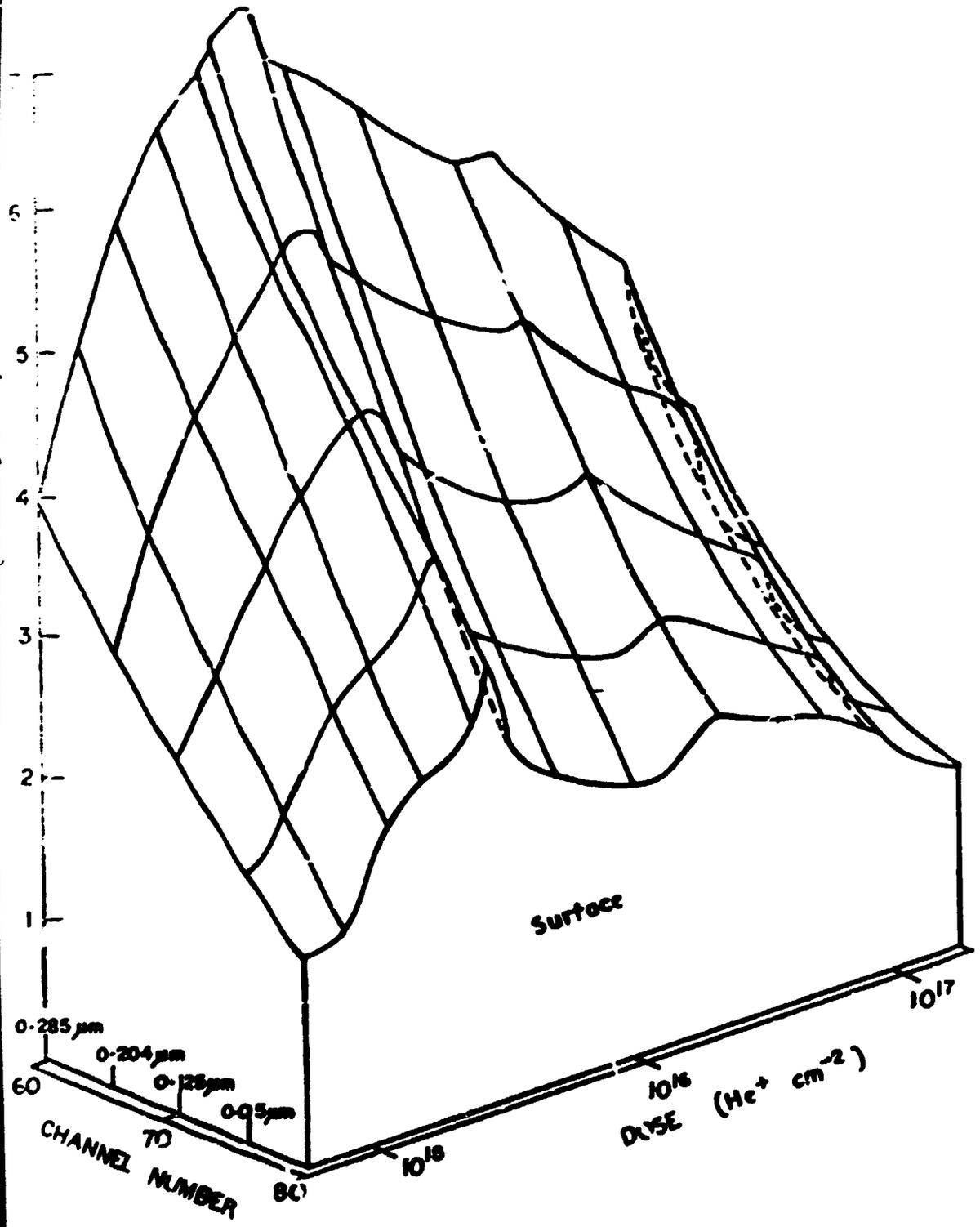

Fig. 3b.

Yield as a function of dose and depth for 1 MeV He^+ in the <100> direction in NaCl. (This work was performed on the A.N.U. 2 MV accelerator and is described in the unpublished thesis of P.B. Price, Ref.11.)

The dose at which this maximum occurs has been found to be temperature dependent and dose rate dependent[12]. It is not known whether such 'annealing' occurs when the solid is bombarded by heavier ions. In alkali halides, 90 MeV ^{12}C ions have approximately the same stopping power as 1 MeV He^{+} ions.

Such an experiment could have certain complications as the energy resolution of detectors for heavy ions is not as good as for light ions, and the yields could be much lower if the beam particles were heavier than the crystal atoms. One proposal to overcome some of these difficulties will be discussed later, §9.

§4. ENERGY LOSS OF IONS, RANGE MEASUREMENTS:

In addition to observing the radiation from excited ions and studies of the channeling effect, another closely related type of experiment in this field is range measurements of heavy ions in both amorphous and crystalline solids[21]. The justification for wanting to measure the range of heavy ions is the recent upsurge in ion implantation studies[20], which is of importance for semi-conductor technology. If one wants to implant semi-conductors with various dopant species, the information on how deep the ions penetrate, radiation damage created, and the location of the ions, is of utmost importance. In nuclear spectroscopy or radiation damage studies, the distance that an energetic recoil atom travels through a solid is one of the important experimental parameters. There are two distinct ways for studying ranges in solids, viz., chemical methods and physical methods, Fig. 4. In the chemical method, implanted radioactive atoms are assayed by removing layers from the surface and measuring their specific radioactivity. However simple chemical etching of the target is not noted for its uniformity or reproducibility. Other chemical methods which are more accurate will not be described here. A corresponding physical method for estimating the depth distribution of implanted radioactive ions is to combine a measured distribution of energies of the outcoming particles, with a previously determined stopping power.

Another way is to implant ions which have a sharp (p,α) resonance and by bombarding the solid with protons of known energies, one detects the outcoming α-particles. By measuring their energy, and knowing the stopping powers of protons and alpha particles, one can calculate the depth distribution.

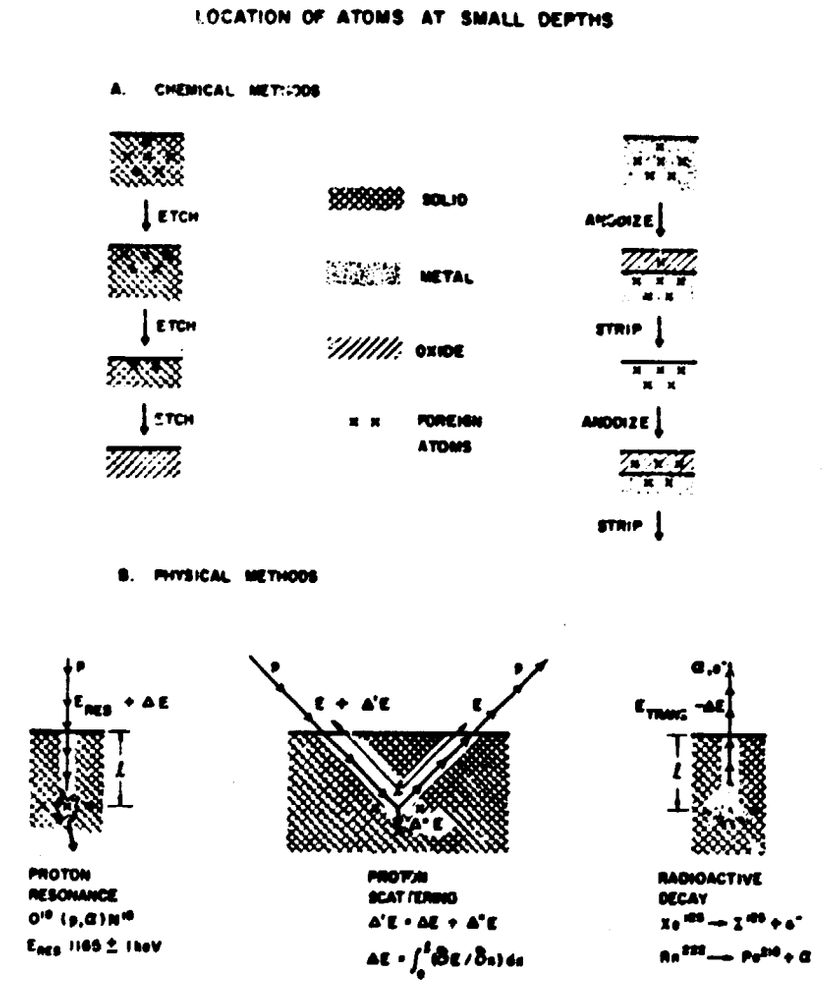

Fig. 4.
Techniques for measuring the depth distribution of foreign atoms at shallow depths in a solid, (Davies, Ref.21)

Rutherford scattering can be used for energy loss measurements. A proton or α-particle, scattering off an atom in the solid, loses energy on the way in, in the collision process, and on the way out. Therefore knowing the proton energy loss on scattering and measuring the outcoming energy one can calculate the depth at which the collision occurred. One can use this technique for pure solids and implanted atoms in solids[22-23], Fig. 5, for very thin targets, determining specific energy loss, and for thick targets, obtaining depth distributions. From the FWHM of the peak

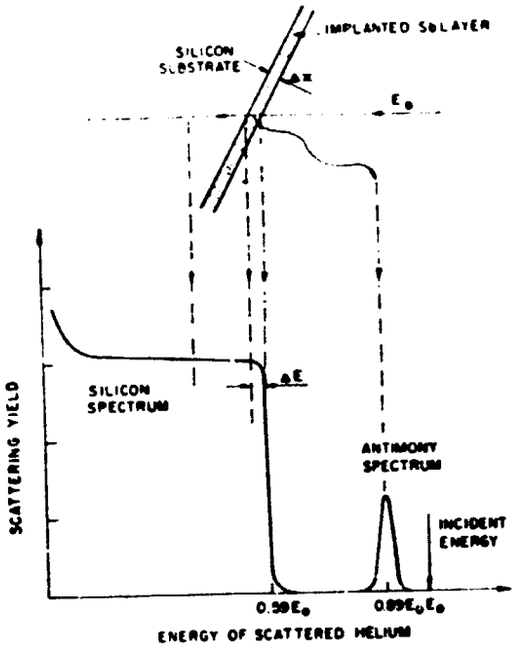

Fig. 5.

Schematic representation of the energy spectrum of a helium beam (incident energy, E_0) backscattered from a thick silicon target in which some heavy atoms (Sb) are embedded at a shallow depth, (Davies, Ref.21)

one can estimate the range straggling. A few range measurements have been undertaken in single crystals and the ranges have been found to differ considerably from measured ranges in amorphous solids. This is due to the channeling mechanism. Since range and stopping power are closely correlated, a few studies have been carried out to measure stopping powers in single crystals, but more studies are needed for a wide range of crystals, particles and energies.

5. OSCILLATORY EFFECTS IN CHANNELING:

One method used for measuring stopping powers is to use thin self-supporting foils of known thicknesses and measure the energy of the transmitted particles.

This last method has been developed considerably at Oak Ridge National Laboratories where a research programme has had the objective of measuring the energy loss of ions transmitted through very thin crystalline foils. Using very thin foils is to ensure the condition that the trajectories of the detected particles do not attain statistical equilibrium while traversing the crystal. From this data it has been possible to derive theoretical interatomic potential parameters. When beams of positive ions are transmitted through thin gold crystals in directions nearly parallel to the more closely packed atomic planes, considerable structure is observed in the spectrum of the transmitted ion energies[24], Fig. 6. The details of the observed spectra are dependent on the distance the ions travel in the crystal, the angular relations between the crystal axis and the directions of the transmitted beam and the detector. If one assumes that the particle is moving in a planar channel consisting of two parallel closely packed lattice planes, it will experience a repulsive force from the atoms in each wall. As the critical angle ψ_c is small, e.g. for 2 MeV He^+ in Si ψ_c is of the order $\sim 1°$, one may approximate the motion by a two dimensional situation in which the direction of incidence into the channel lies in the xz plane and the z component of the velocity can be assumed constant, so that

$$\frac{d^2x}{dz^2} = -\frac{1}{2E}\frac{\partial V(x)}{\partial x} \quad , \qquad 3.$$

where E is the particle energy. Datz et al.[24] expressed the potential V(x) in the form

$$V(x) = V(o) + a_1 x^2 + b_1 x^4 + \ldots \quad , \qquad 4.$$

in which case the equation of motion is that of an undamped anharmonic oscillator. Thus the structure in the spectra has been ascribed to particles that have made an integral number of oscillations in the crystal, as is shown in Fig. 7. By choosing the geometry of the experiment carefully, the detector subtending a small angular aperture, only particle trajectories with wavelengths given by the boundary conditions

$$\lambda_a = (L \pm z_o \mp z_e)/n \quad , \qquad 5a.$$

$$\lambda_{b'} = (L + z_o + z_e)/(n + \tfrac{1}{2}) \quad ,$$

$$\lambda_{b''} = (L - z_o - z_e)/(n + \tfrac{1}{2}) \quad , \qquad 5b.$$

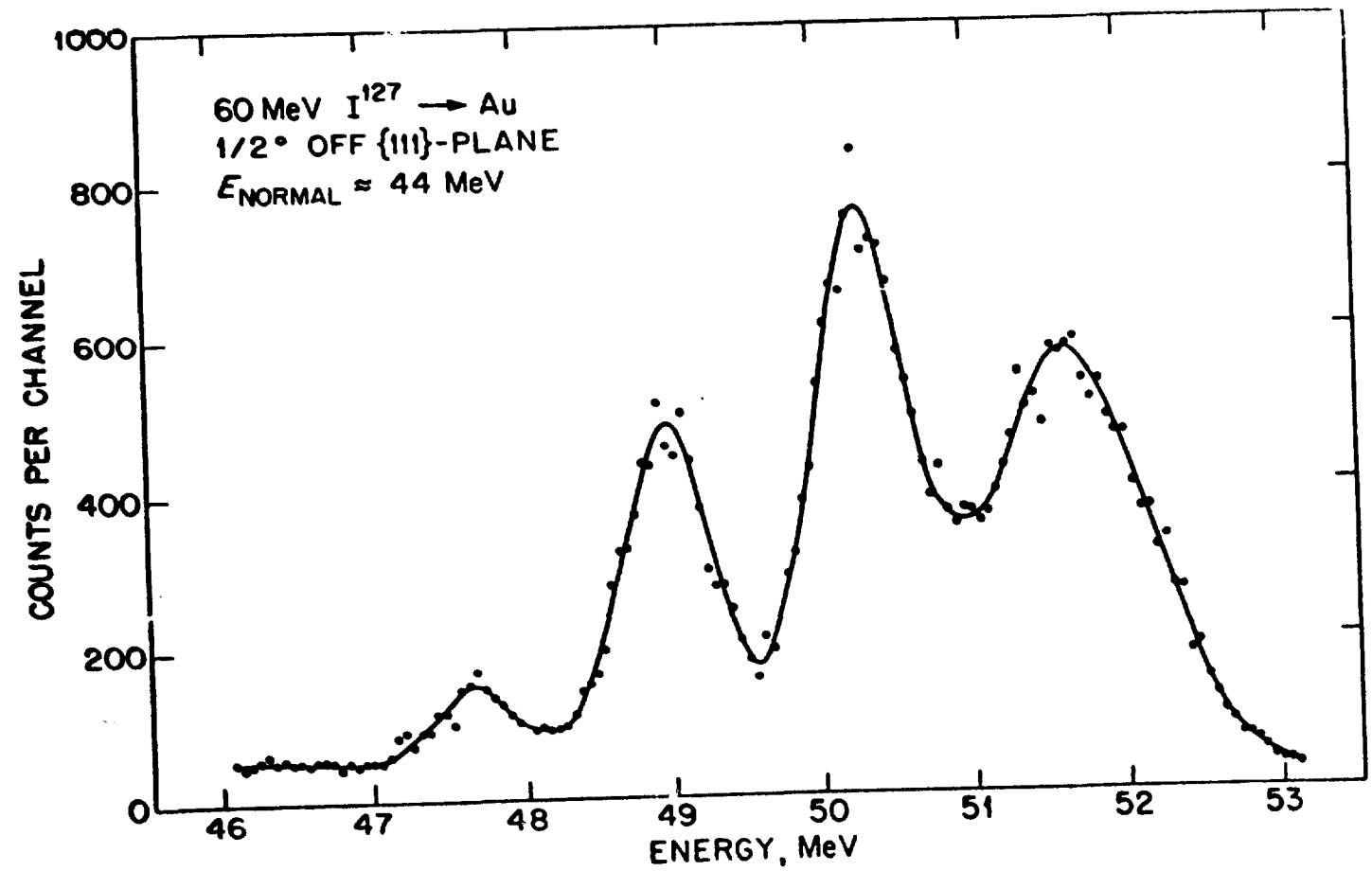

Fig. 6.

Magnetic deflection spectrum (recorded with a position sensitive detector) of 60 MeV ^{127}I passing through 0.7 μm of Au. The detector is in line with the beam direction and the crystal is tilted 1/2° from a {111} plane. The energy of a particle after traversing the crystal in a random direction is 44 MeV, (Datz et al., Ref.24)

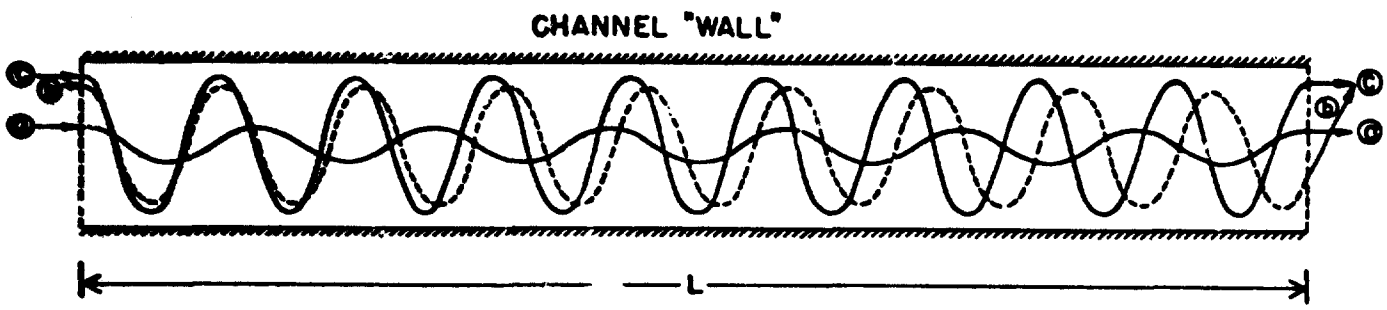

Fig. 7.

Trajectories for three entrance points. Particles a and c will reach a detector in line with the beam, (Datz et al., Ref.24).

will be detected. n is an integer, L is the traversed thickness of the crystal, and z_o and z_e are the lengths associated with the phase shifts of incidence angle ψ_o and exit angle ψ_e. This is illustrated in Fig. 8.1 and Fig. 8.2. The fact that several values of n can contribute to the energy spectrum is due to the anharmonic nature of the interplanar potential. The closer the ions move to the "channel wall" the greater repulsion it experiences, therefore the trajectories will have shorter wavelengths and larger amplitudes, which implies a larger average stopping power. As the geometry of the experiment selects quantized values of λ_a and λ_b, one has the reason for the discrete peaks observed in the transmitted particle spectrum. Choosing experimentally $\psi_o = \psi_e = 0$ then

$$\lambda_z = L/n \quad , \qquad 6a.$$

$$\lambda_b' = \lambda_b'' = L/(n + \tfrac{1}{2}) \quad . \qquad 6b.$$

If one then changes the pathlength, i.e. the effective thickness of the target by rotating the crystal about a suitable axis, so that the energy loss for "peak n + 1" is equivalent to the previously measured "peak n", one has that $\lambda_n = \Delta T$, the change in the effective thickenss. One can then determine n from 6a. Tilting the crystal plane with respect to the beam axis splits the λ_b solutions, but the λ_a solutions are unchanged so long as the detector is on the beam axis. From this one can understand that mosaic spread in single crystals will give a spread in the incident angle ψ_o which will smear out the values of λ_b, but will not affect λ_a. Therefore one will only obtain discrete peaks for the λ_a trajectories.

The Oak Ridge National Laboratory group has performed experiments[25] for 15-22 MeV ^{127}I-ions and 60 MeV ^{127}I-ions, 10 MeV ^{16}O-ions and 3 MeV ^{4}He ions on gold and silver single crystals of <111> and <100> orientations, using different methods of detection. These used time of flight analysis or magnetic analysis, Fig. 9. All the data, when corrected to the incident beam energy, exhibited a linear relationship between the stopping power and the corresponding channel oscillation frequency, Fig. 10a, b.

$$\left(-\frac{dE}{dx}\right)_{E_o} = \alpha + \beta\omega \quad , \qquad 7.$$

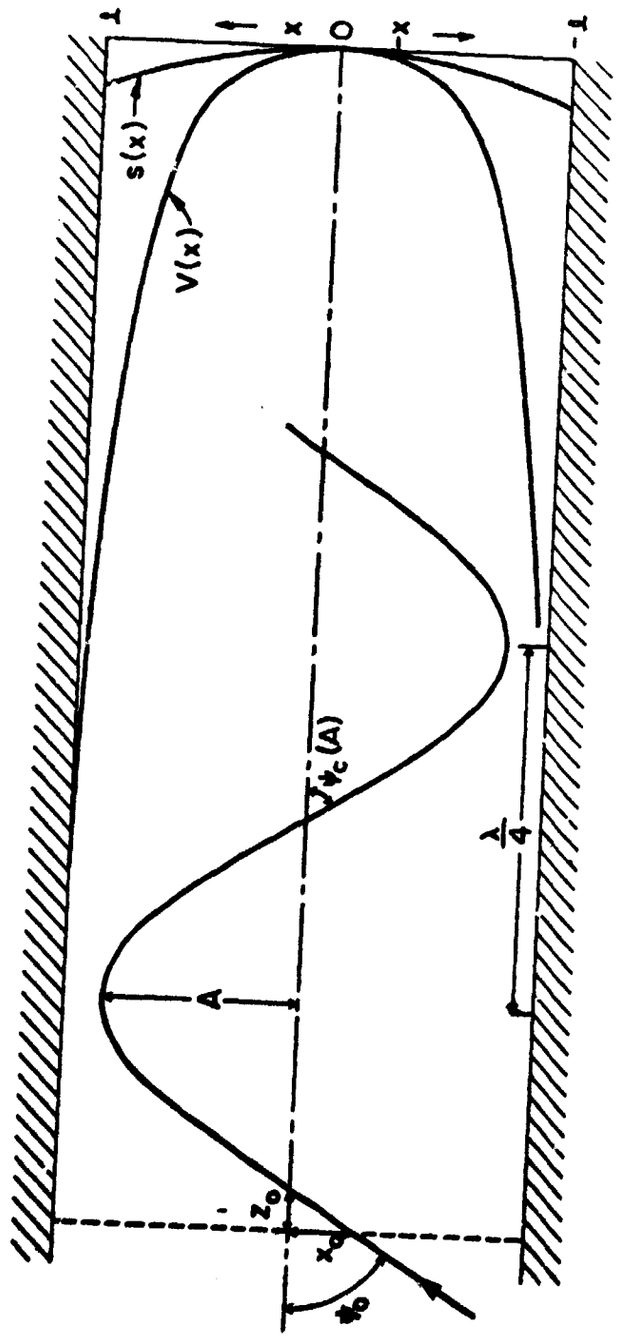

Fig. 8.1. Trajectory of an ion entering a planar potential at x_o and angle ψ_o. The potential V(x) and stopping power S(x) functions are indicated on the right, (Datz. et al.,Ref.24).

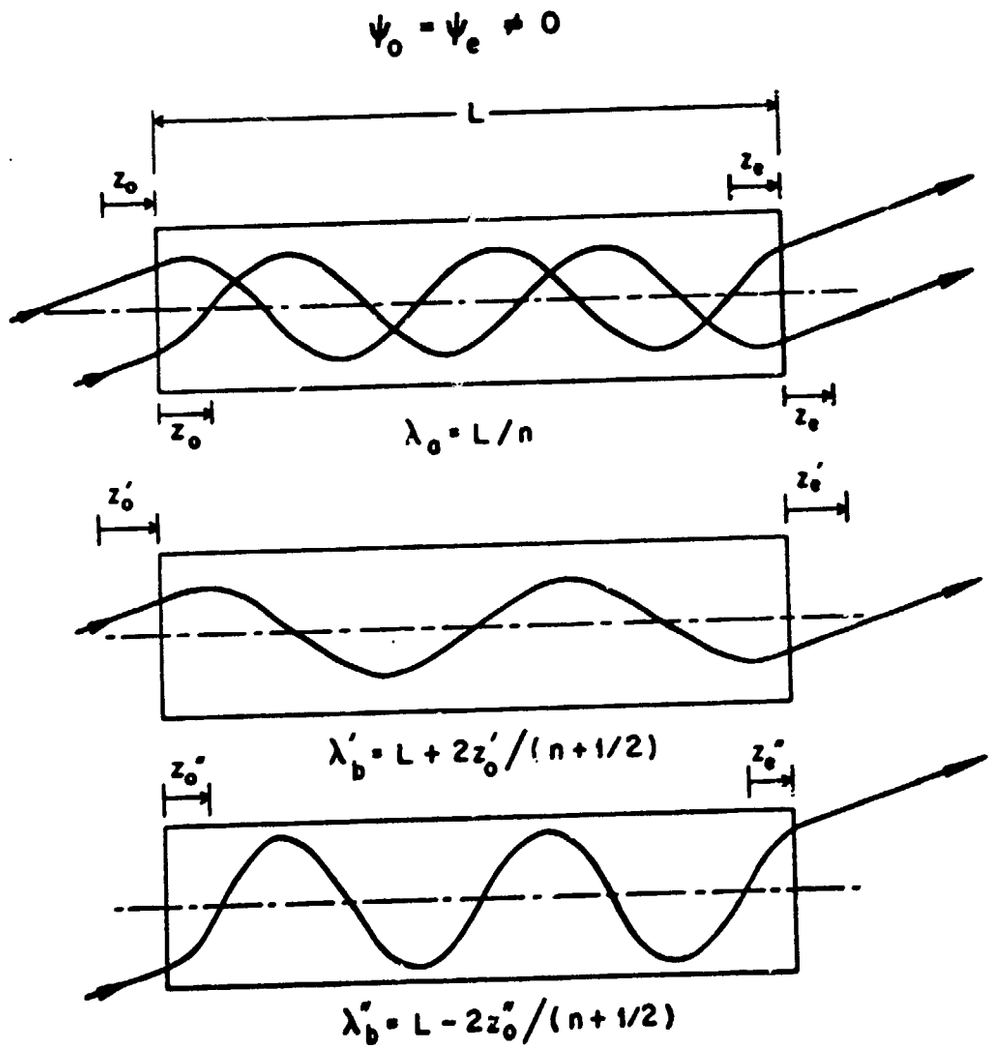

Fig. 8.2.

Trajectories demonstrating four solutions of eqs. 5(a,b) for $\psi_o = \psi_e \neq 0$. The solutions to eq. 5a (λ_a) are degenerate in wavelength. The solutions for eq. 5b (λ_b' and λ_b'') give wavelengths longer (λ_b') and shorter (λ_b'') than eq. 5a., (Datz et al., Ref.24).

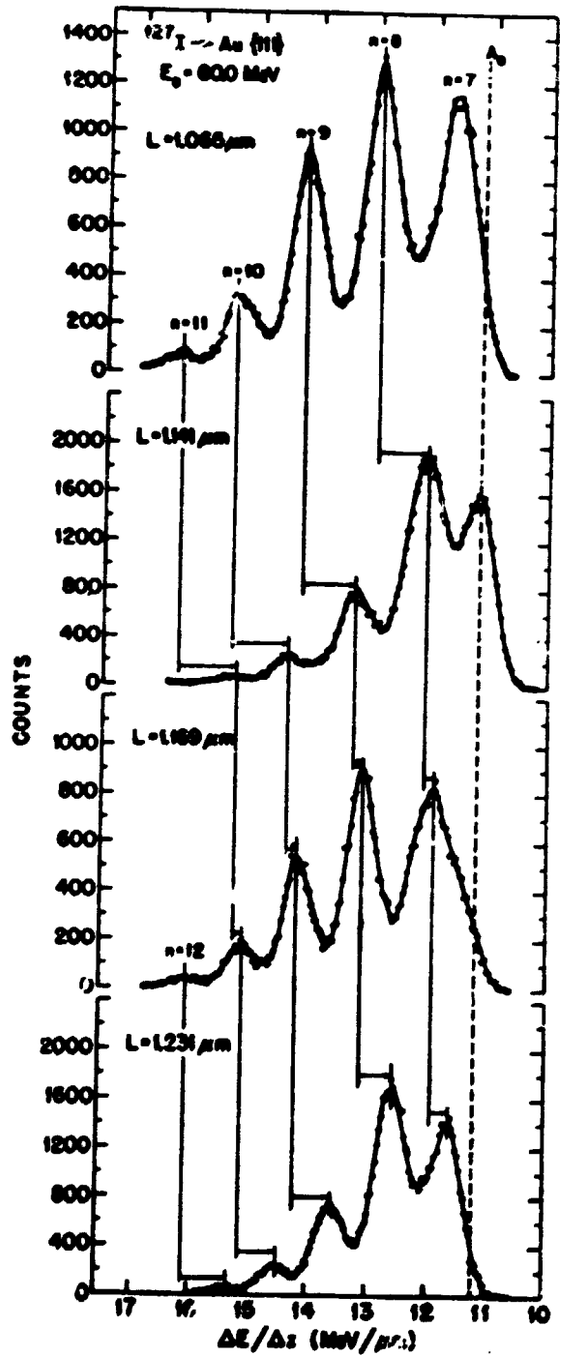

Fig. 9.

Energy loss spectra of 60 MeV ^{127}I ions channeled in a (111) plane of Au as a function of path length (time of flight analysis, Datz et al., Ref. 24).

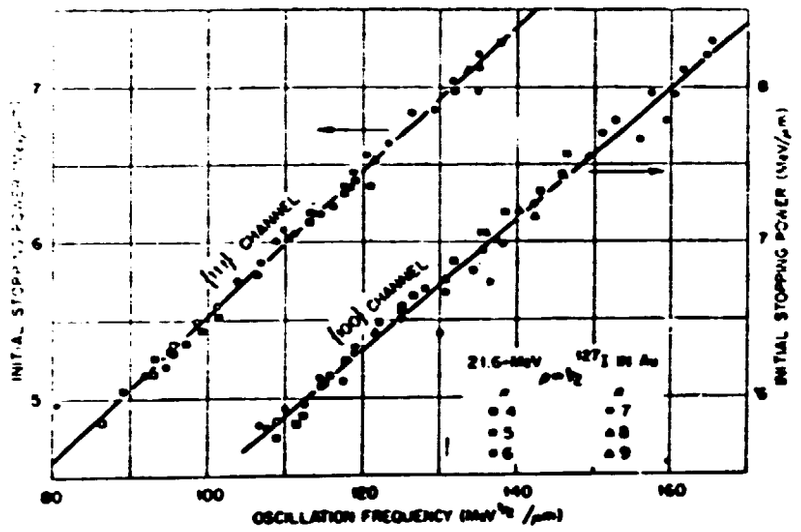

Fig. 10a.

Initial stopping power as a function of channel oscillation "frequency" for 21.6-MeV ^{127}I ions in the {111} and {100} channels of gold. The stopping-power energy exponent was assumed to be 1/2. (Datz et al.,Ref.24)

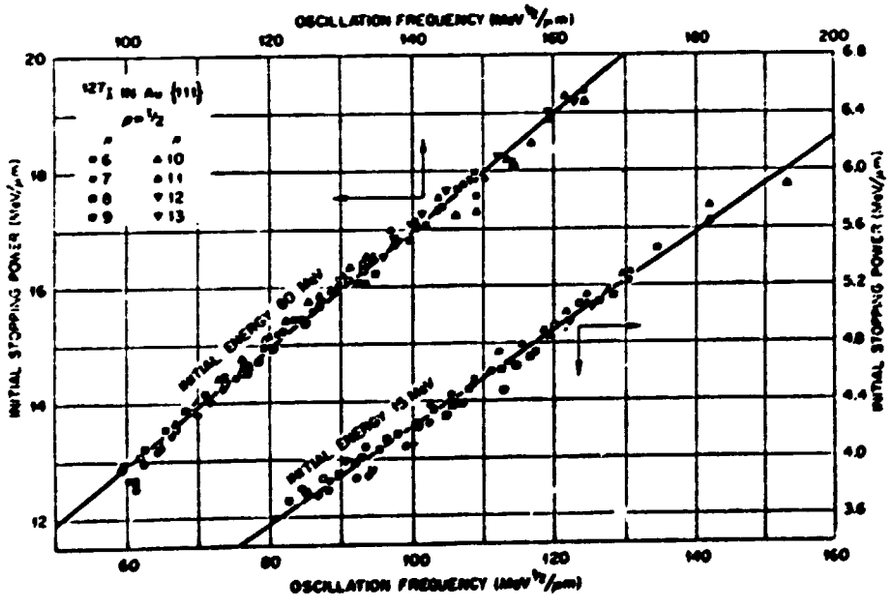

Fig. 10b.

Initial stopping power as a function of channel oscillation "frequency" for 15- and 60-MeV ^{127}I ions in the {111} channel of gold, (Datz et al., Ref.24).

where α and β are empirical constants. The most important feature of this type of experiment is that one is able to extract atomic and planar potentials from the measured data, as has been proposed by M.T. Robinson[26]. Using the assumption that the stopping power can be expressed as

$$S(x,E) = S_0 + S_1 \{\sigma(x)-1)\} , \qquad 8.$$

where S_0 and S_1 depend on energy, he found that α and β could be expressed as

$$\alpha = S_0 - S_1 , \qquad 9.$$

$$\beta = 2S_1 \int_0^{x_m} \sigma(x) \{V_2(x_m) - V_2(x)\}^{-1/2} dx , \qquad 10.$$

where

$$V_2(x) = V_1(\ell+x) + V_1(\ell-x) \; ; \; -\ell \leq x \leq \ell , \qquad 11.$$

and $V_1(\underline{x})$ is defined as follows:

$$V_1(\underline{x}) = 4\pi\kappa\rho\ell \int_{\underline{x}}^{\infty} r\, V(r) dr . \qquad 12.$$

V(r) is the interatomic potential between an ion and a lattice atom, r is the distance, ρ is the target atomic density and ℓ is the half width of the channel, $\underline{x}$ is the length of the normal from the ion to the plane and κ expresses the possibility of different channel widths. The experimental data may be used to evaluate the curvature of the potential

$$y \equiv 2\pi^2 (S_0-\alpha)^2/\beta^2\ell = -8\pi\rho\kappa\{V(\ell) + \ell V'(\ell)\} . \qquad 13.$$

As a check one can calculate the amorphous solid stopping power from these parameters and compare it with the measured "random" stopping power. If the interaction potential between the channeled ion and the individual lattice atoms is of the screened Coulomb form, the curvature parameter is

$$y = -8\pi\rho\, Z_1 Z_2 e^2 b\phi'(b\ell) , \qquad 14.$$

where Z_1e and Z_2e are the effective nuclear charges, $\phi'(b\ell)$ is the screening function and b is a constant. By measuring the stopping power for two

different orientations one can obtain the value for b, see Table 2.

TABLE 2

Curvature parameters observed for ions moving in the planar channels of gold crystals, (Datz et al.,Ref.24).

Ion	Energy (MeV)	Curvature parameter (eV/Å²) γ_{111}	γ_{100}	Ratio $\gamma_{111}/\gamma_{100}$	Screening constant b* (Å⁻¹)
[illegible]	3	64.0 ± 2.8	108.1 ± 5.8	0.592 ± 0.041	3.32 ± 0.44
[illegible]	10	154.4 ± 8.9	253 ± 29	0.610 ± 0.078	3.12 ± 0.82
[illegible]	15	837 ± 48	...	...	...
	21.6	915 ± 53	1600 ± 114	0.572 ± 0.053	3.55 ± 0.58
	60	1288 ± 50	2077 ± 92	0.620 ± 0.037	3.03 ± 0.37
			Weighted mean:	0.604 ± 0.017	3.22 ± 0.18

*For a hyperbolic cosine planar-channel potential $b = [\ln(\gamma_{111}/\gamma_{100})]/(\theta_{100} - \theta_{111})$. For Au, $\theta_{100} = 1.0197$ Å and $\theta_{111} = 1.1774$ Å.

M.T. Robinson[26] considered several potentials and found that the data agreed very well with the Hartree potential[27], whereas the other potentials gave too large screening lengths.

Gibson and Golovchenko[28] have proposed a method for detecting the planar continuum potential from the channeling data without having to assume a stopping power expression. Their method is based on the fact that the form of the potential may be deduced from the knowledge of the oscillation period as a function of the "transverse energy" $E_\perp = E\sin^2\psi \simeq E\psi^2$, as ψ is small. The transverse energy associated with a given detected wavelength is found by keeping the traversed thickness T of the crystal constant and varying ψ_o, which changes the population of the different energy loss peaks. With 1.8 MeV He^+ on Au[28], ψ_o was varied to find the position for maximum population in a particular energy loss group summed over all charge states. The transverse energy for that group was then found from $E_\perp = E\psi^2_{o,n}$, n specifying the group. By choosing a function for λ which gave the best fit to the experimental data, they were able to obtain the inverse of the potential from the transformation[29]

$$x(U_2) = (8\pi^2 M_1 V^2)^{-1/2} \int_0^{U_2} \lambda (U_2 - E_\perp)^{-1/2} dE_\perp \quad . \qquad 15.$$

The function for λ that Gibson and Golovchenko chose gave the potential

$$U_2(x) = \tfrac{1}{2}a_1 x^2 + \tfrac{1}{4}a_2 x^4 \quad , \qquad 16.$$

and the results agreed with the Oak Ridge results. Since this method has only been applied to one case more experimental studies with a variety of ions, energies and targets are required. Using very energetic heavy ions would reduce problems of radiation damage in the crystalline targets.

6. X-RAY PRODUCTION IN SOLIDS

For the trajectories that have the larger amplitudes, implying that their distance of closest approach to the lattice atoms is smaller, one would expect a larger X-ray yield from both the projectile and the target atoms. A further development in these measurements would be to observe the X-ray yield in coincidence with specific energy loss groups. From the data of Datz et al., see Table 2, the screening length b does not vary very much with energy, so it would be of interest to perform X-ray coincidence experiments with varying projectile energy. A recent letter[30] in the literature reports of a coincidence experiment between X-rays generated and specific energy loss groups in the 60 MeV ^{127}I on Au crystals. A time of flight analysis similar to the ORNL experiment was performed. The characteristic X-ray production $\bar{p}$ was found from

$$\bar{p} = f \cdot N_X/N \quad , \qquad 17.$$

where f is an efficiency factor, N_X is the number of detected X-rays and N is the number of ions of a specific energy loss. $\bar{p}$ was then reduced to the X-ray production per one oscillation in the crystal

$$\bar{p}_\lambda = \bar{p}/n \quad , \qquad 18.$$

n being the number of oscillations. The results are shown in Fig. 11. From the data a total X-ray excitation cross section can be calculated. The results show that the Au M shell excitation cross section is too small by a factor ~ 5 compared to other experiments. The reason is believed to be due to the fact that collisions where $\rho \leq 0.1$Å were avoided in the experiment. The data seems to indicate that there is some structure in the measured X-ray production.

There are at least 3 aspects of these experiments that warrant further investigation, as they have not been mentioned previously, namely coherent excitation, measurements of energy loss spectra of specific charge states of the transmitted ions and non-characteristic X-ray bands which

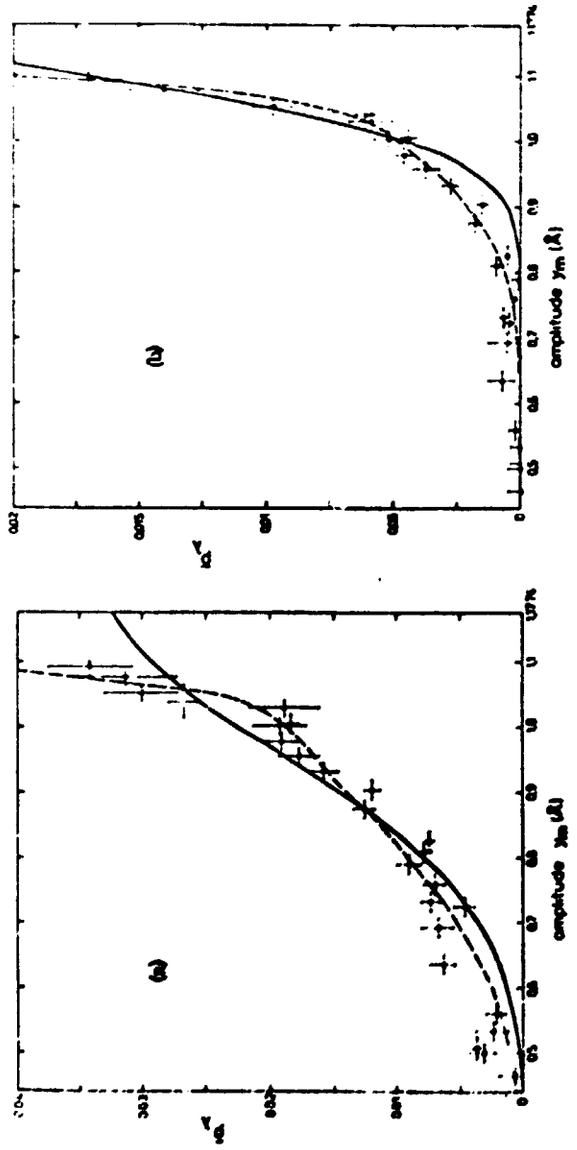

Fig. 11. Characteristic X-ray production $\bar{p}_\lambda$ in the system I + Au(111) as a function of ion oscillation amplitude y_m. The data points are reduced to a uniform ion energy of 50 MeV. Crystal thickness: circles, 3000-5500 Å ; triangles, 5500-6800 Å. Solid and dashed curves are least-squares fits. (a) Au M excitation, (b) I M excitation, (Ambros et al., Ref.30).

have been observed recently and reported in the literature[32-34].

§7. COHERENCE EFFECTS IN CHANNELING:

Okorokov et al.[31] performed an experiment in which coherent excitation of atoms moving through a single silver crystalline target was observed. The effect was described as a resonant atomic excitation when the transition frequency ν,

$$\nu = (E_{exc}-E_{gs})/h, \quad \text{is equal to the}$$

frequency of the collision for the atom passing through the crystal, that is:

$$\nu_c = \nu = V_o/d. \qquad 19.$$

where V_o is the particle velocity, d is the distance between atoms in the crystal. They measured the intensity of the 4685Å transition in HeII after He^+ ions had traversed a thin single crystal of silver. They observed a resonance in the intensity when the ion energy minus the energy loss in the crystal satisfied eq.19, implying that the excitation occurs in the last few layers of the target. For ^{127}I MeV ions in gold one could expect similar effects for energies up to 200 MeV.

This experiment needs to be done on the 14UD accelerator to investigate the effect of this excitation process on the previously-mentioned energy loss - X-ray coincidence experiment.

In the time of flight measurements of the energy loss through single crystals, Datz et al.[24] did not observe the charge state distribution of the emergent ions, due to the experimental configuration, but in the magnetic analysis, structure was observed in the energy spectrum of each charge state. They used a multicomponent beam which was magnetically analyzed and they detected the transmitted ions in a solid state detector. These experiments should be combined to use ions of a single charge state and analyze the transmitted beam by means of a velocity filter[35], e.g. a combined electric and magnetic analyzer. Other things being equal the ability of achieving even higher energies of ions in this department would decrease the rate of radiation damage in the crystal.

8. FORMATION OF UNITED ATOMS

Ambros et al.[30] did not mention in their article whether they observed any non-characteristic X-ray bands whereas Mokler et al.[34] have bombarded targets of Au, Th and U with 10-60 MeV I ions and reported X-ray bands at 8.2, 9.5 and 9.8 keV respectively. Since these bands could not be due to contaminations, and the peak positions coincided, within 200 eV, with extrapolated transition energies for $M_{\alpha_{1,2}}$ X-rays of the corresponding superheavy atoms, the bands were tentatively assigned as X-rays from the united atom, formed by the overlap of the projectile and target atoms.

There are two proposed theoretical mechanisms to describe the creation of inner shell excitations. Two distinct types of mechanisms are Coulomb excitation and Pauli-excitation[36], i.e. electron promotion. Projectiles that act as bare charged point particles produce holes in inner shells of target atoms, via Coulomb excitation. Projectiles that carry a coterie of electrons into the interaction region promote inner shell electrons by virtue of the Pauli exclusion principle acting in the overlapping electron clouds of the colliding partners. For suitable projectile energies, a "quasimolecule", or "united atom" is formed during deeply penetrating collisions and under appropriate circumstances, greatly enhanced K X-ray yields can be observed from the lighter collision partner, especially when energy-level matching occurs. These larger yields are often due to a transfer of a K-shell electron in the lighter collision partner to an unoccupied level in a shell of higher principal quantum number (often the L-shell) in the heavier collision partner. The K-shell ionization cross sections under Pauli excitation conditions are larger by orders of magnitude than the Coulomb-ionization cross sections at the same projectile velocities. Extensive studies both theoretical and experimental have been performed in the last few years. For symmetrical cases such as Ne^+ - Ne and Ar^+ - Ar[37], as shown in Fig. 12, theoretical and experimental results have agreed fairly well, but in asymmetrical cases the theoretical predictions do not agree with the experimental results. Z-dependence[38] and charge dependence[39] and impact parameter dependence[40] measurements of the X-ray yield have been carried out in the region where Coulomb excitation takes place and also the region where Pauli excitation takes place. Fine structure has been observed[41] in the K X-rays which has been attributed to the simultaneous production of a number of vacancies excited by the projectile.

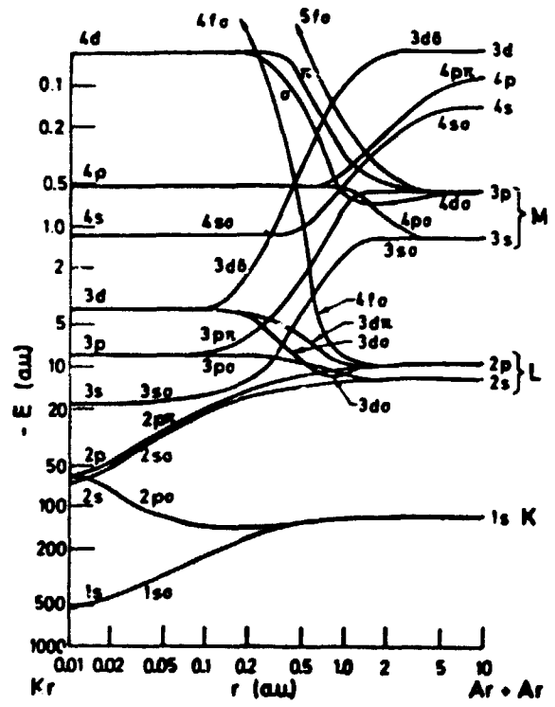

Fig. 12.
Semi-quantitative energy levels for the diabatic, one-electron molecular orbitals of the Ar-Ar system, (Lichten, Ref. 36).

§9. PROPOSAL:

The 2 MeV work is proceeding on a well defined project, as has already been described in §3, but it needs to be extended to higher energies. In this section proposals are put forward to accomplish this. The equipment on beam line 2 of the 2 MV accelerator has been designed so that it meets the requirements of vacuum, cleanliness, and beam line height that are necessary on the 14UD accelerator.

9.1. Initially, one could carry the existing equipment between beam line 2 of the 2 MV accelerator and beam line 7, for example, of the 14UD accelerator. This would involve removing a temporary brick wall and performing alignment procedures for each move, which would waste much time and effort if it was necessary to make such moves frequently.

An alternative possibility would be to rearrange the 2 MV accelerator area and place the target chamber at the intersection of a

2 MV beam line and line 7 of the 14UD system. Thereafter it would only be necessary to rotate the scattering chamber approximately 60° to the appropriate beam line.

9.2. The final objective would be to incorporate a magnet, placed at the intersection of the two beam lines, Fig. 13, e.g. the 60° double focussing magnet, stored in Engineering Physics, which would need magnet box modification to add a straight through port and its vacuum properties checked.

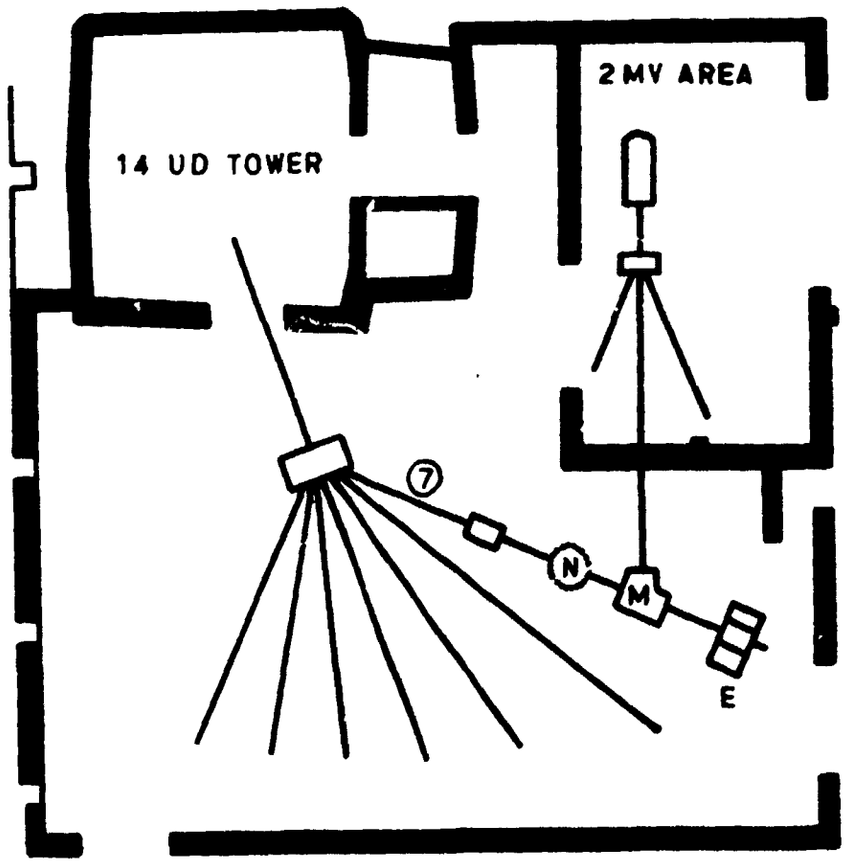

Fig. 13.

Proposal for a 2 accelerator system. M is a bending magnet, E is the equipment presently on beam line 2 of the 2 MV accelerator and N is possible nuclear physics equipment. The angle between the 2 beam lines is ∿ 60°. (The positions M and E are very close to the service trench but neither will prevent access.)

Placing the equipment at the end of beam line 7 would enable the line of research currently in progress on the 2 MV accelerator (§3) to continue and to be extended to higher excitation energies with heavy ions. This also permits studies of the interaction of very energetic ions in solids at energies which have not been available previously. It is envisaged that following this work, the next most promising line of research would be that on oscillatory effects in solids using energetic heavy ions (§5).

Situating the equipment at the end of the beam line would not interfere with any nuclear physics equipment further up the beam line, provided it did not require a permanent beam dump. Equipment has either been developed or bought to enable studies of most of the abovementioned topics: three-axis goniometer, Si(Li) detector, beam-foil translation state, high voltage analysis equipment, etc. Data acquisition[42] has likewise been developed on the IBM 1800 which would be applicable to experiments performed on the 14UD accelerator. The two accelerator system would be very advantageous to ion implantation studies (§4), using the 14UD accelerator to implant energetic heavy ions into a solid, and a proton beam from the 2 MV accelerator to probe depth distributions, atom location studies of the implanted ions, and radiation damage in the solid.

REFERENCES

1) G.W. Carriveau, Ph.D. Thesis, A.N.U. 1972, unpublished.

2) Proceedings of the Second International Conference on Beam-Foil Spectroscopy, Nucl. Instr. & Meth. 90 (1970).

3) W.L. Wiese, Nucl. Instr. & Meth. 90 (1970) 25.

4) M. Leventhal, Nucl. Instr. & Meth. 110 (1973) 343.

5) S.R. Lundeen, Y.L. Yung & F.M. Pipkin, Nucl. Instr. & Meth. 110 (1973) 355.

6) I.A. Sellin, Nucl. Instr. & Meth. 110 (1973) 477.

7) D.J. Pegg, P.M. Griffin & I.A. Sellin, Nucl. Instr. & Meth. 110 (1973) 489.

8) C.L. Cocke, B. Curnutte & J.R. Macdonald, Nucl. Instr. & Meth. 110 (1973) 493.

9) P. Richard, R.L. Kauffman, F.F. Hopkins, C.W. Woods & K.A. Jamison, Phys. Rev. Letts. 30 (1973) 888.

10) C.L. Cocke, B. Curnutte & J.R. Macdonald, Phys. Rev. Letts. 28 (1972) 1233.

11) P.B. Price, Thesis, Univ. of N.S.W. 1973, unpublished.

12) M.J. Hollis, Phys. Rev. B8 (1973) 931.
M.J. Hollis, C.S. Newton & P.B. Price, Phys. Lett. 44A (1973) 243.

13) R.S. Nelson,"The Observation of Atomic Collisions in Crystalline Solids" North Holland Publishing Company (1968)

14) Channeling, D.V. Morgan (Editor), John Wiley & Sons (1973)

15) D.S. Gemmell, Rev. Mod. Phys. 46 (1974) 129.

16) W.M. Gibson, B.N.L. 50336, Feb. 1973.

17) Atomic Collision Phenomena in Solids, Editors: D.W. Palmer, M.W. Thompson & P.D. Townsend, North Holland Publishing Company (1970).

18) Atomic Collision in Solids^{IV}, Editors: S. Anderson, K. Bjorkqvist, B. Domeij & N.G.E. Johansson, Gordon and Breach Science Publishers (1972).

19) W. Brandt, Scientific American, 91, March 1968.

20) Ion Implantation, G. Dearnaley, J.H. Freeman, R.S. Nelson & J. Stephen, North Holland Publishing Company (1973).

21) J.A. Davies, IAEA-SMR-8/51 and references quoted therein.

22) e.g. W.K. Chu, J.F. Ziegler, I.V. Mitchell & W.D. Mackintosh Appl. Phys. Lett. 22 (1973) 437.

23) J.F. Ziegler & M.H. Brodsky, J. Appl. Phys. 44 (1973) 188.

24) S. Datz, B.P. Appleton & C.D. Moak, Chapter VI, Ref. 14.

25) Ref.24 and references quoted.

26) M.T. Robinson, Phys. Rev. 179 (1969) 327, and Phys.Rev. B4 (1971) 1461.

27) T.C. Tucker, L.D. Roberts, C.W. Nestor Jr., & T.A. Carlson Phys. Rev. 178 (1969) 998.

28) W.M. Gibson & J. Golovchenko, Phys. Rev. Lett. 28 (1972) 1301.

29) L.D. Landau and E.M. Lifshitz, Mechanics (Pergamon, New York, 1960) p.27.

30) R. Ambros, H.O. Lutz and F. Reichelt, Phys. Rev. Letts. 32 (1974) 811.

31) V.V. Okorokov, D.L. Tolchenkov, I.S. Khizhnyakov, Yu. N. Cheblukov, Yu. Ya. Lapitsky, G.A. Iferov & Yu. N. Zhukov, Phys. Letts. 43A (1973) 485.

32) J.R. Macdonald and M.D. Brown, Phys. Rev. Letts. 29 (1972) 4.

33) W.E. Meyerhof, T.K. Saylor, S.M. Lazarus, W.A. Little, B.B. Triplett & L.F. Chase Jr., Phys. Rev. Lett. 30 (1973) 1279, and Phys. Rev. Lett. 32 (1974) 1279.

34) P.H. Mokler, H.J. Stein, & P. Armbruster, Proceedings of the International Conference on Inner Shell Ionization Phenomena, Atlanta, 1972, p.1283.

35) L. Wåhlin, Nucl. Instr. & Meth. 38 (1965) 133.

36) U. Fano & W. Lichten, Phys. Rev. Letts. 14, (1965) 627,
W. Lichten, Phys. Rev. 164 (1967) 131.

37) F.P. Larkins, J. Phys.B 4 (1971) 1; 4 (1971) 14;
Phys. Rev. A5 (1972) 2288 and J. Phys. B 6 (1973) 1566.

38) D. Burch, N. Stolterfoht, D. Schneider, H. Wieman & J.S. Risley
Phys. Rev. Letts. 32 (1974) 1151.

39) J.R. Mowat, I.A. Sellin, D.J. Pegg, R.S. Peterson, M.D. Brown and J.R. Macdonald, Phys. Rev. Letts. 30 (1973) 1289.

40) C.L. Cocke & R. Randall, Phys. Rev. Letts. 30 (1973) 1016.

41) P. Richard, W. Hodge & C.F. Moore, Phys. Rev. Letts. 29 (1972) 393.

42) Program POLLY, H.J. Hay, A.N.U.
Program MULTI, H.J. Hay & D.F. Hebbard, A.N.U.